Defect and Diffusion Forum Vols. 261-262 (2007) pp. 109-126
online at http://www.scientific.net

Diffusion of molecules at the interface of water-membrane structures

Ye.V. Tourleigh[a], K.V. Shaitan[b] and N.K. Balabaev[c]

Moscow State University, Leninskie gory,

Moscow, 119992

Russia

[a]yegr@moldyn.ru, [b]shaitan@moldyn.ru, [c]balabaev@impb.psn.ru

Key words: molecular dynamics, membranes, diffusion.

Abstract. The distributions and transfer energies of several molecules and atomic groups between water and a structured hydrophobic phase were calculated by the molecular dynamics method. The coefficients of oxygen diffusion in a tetradecane membrane were estimated. The transfer energy of charged atomic groups was found to correlate with changes in the Born solvation energy. The contributions of atoms to the transfer energy of functional groups were shown to be non-additive. The steered dynamics method for estimating the kinetic parameters of the penetration of molecules through interphase boundaries was developed. Heterogeneous microviscosity of a membrane was calculated for a hydrated l-palmitoyl-2-oleoyl-*sn*-glycero-3-phosphatidylcholine bilayer. Effects of the chemical properties of penetrant molecule on its translocation through the membrane were studied.

Introduction

The molecular dynamics (MD) of heterogeneous and membrane structures is currently of great interest and is used in fundamental studies of the dynamic behavior of such systems. Detailed experimental investigation of local physicochemical properties and dynamics of biological membranes is also of considerable interest but attended with certain difficulties [1, 2]. This is especially true for the microscopic picture of mass and energy transfer in strongly anisotropic structured heterogeneous media, the formation and relaxation of non-equilibrium supramolecular structures, and the special features of the distribution of molecular groups with different polarities at interphase boundaries. In this work, the molecular dynamics method involving the use of full-atomic force fields, special procedures, and fairly long trajectories is used to refine the microscopic picture of diffusion processes at the boundary between aqueous and membrane phases [3-5].

Extensive studies of the dynamics of biological membranes [6-9] and protein-membrane complexes raises the question of the optimization of computing procedures and modeling membrane structures by some hydrophobic medium [10]. There are comparatively simple models of a virtual hydrophobic medium [11]. The parameters of changes in the energy of groups in the transfer from water to a membrane are determined from the equilibrium constants in the water-octanol system in these models [10, 11]. The method of molecular dynamics allows the distribution functions of molecular groups in a water-membrane system to be calculated and possible non-additive defects estimated.

Studies concerned with the diffusion of small molecules in membranes consisting of both biolipids and simpler organic compounds [12] usually fail to completely track the passive transmembrane transport of even very small molecules such as water, oxygen, ethanol, ammonia, and potassium and chlorine ions. In this work, we calculated the dynamics of several types of molecules, real and biologically important on the one hand and model (Van der Waals spheres) on the other, for the example of a hydrated hydrocarbon membrane. To maintain constant temperature conditions, we used a collisional thermostat [13-15], which does not lead to nonlinear attractor regimes distorting statistical equilibrium in energy distribution over degrees of freedom [16, 17].

As an example of more complex structure, lipid bilayer was investigated in much the same way as the first membrane. In addition, to estimate the microviscosity of the lipid membrane in various parts of the anisotropic bilayer, as well as to study how the structure of penetrants affect their interactions with the membrane, a modified variant of steered molecular dynamics (SMD) was developed [18, 19]. SMD makes it possible to quantitatively estimate parameters, which characterize the physical mechanisms of elementary actions of mass transfer in microheterogeneous structures [20]. This method also allows several complete transfers of the penetrating molecule under study through a membrane to be calculated with reasonable time expenditures.

Objects and methods

The molecular dynamics was calculated with the PUMA software package [21], which was specially modified to include SMD. The system of classical equations for atom movement was solved in the Amber 1999 force field [22].

We calculated membranes consisting of *n*-tetradecane $C_{14}H_{30}$ mono- and bilayers. The cell for calculations contained 24 tetradecane molecules per monolayer (Fig. 1*A*). Periodic boundary conditions were used. The initial structure corresponded to the perpendicular orientation of the axis of the largest extension of molecules with respect to the plane of the membrane. The hydrocarbon density in calculations at constant volume and temperature was of 0.707 to 0.771 g/cm^3 depending on the cell size (the experimental density of the volume phase is 0.761 g/cm^3 under normal conditions).

The partial atomic charges in tetradecane were estimated according to Mulliken using the unrestricted Hartree-Fock method with the 6-31G* basis set. The charges accepted in our calculations are shown in Fig. 1*B*. An ordered membrane structure was formed using a parabolic potential that connected the tetradecane terminal carbon atom to a fixed plane. For the bilayer, there were two such planes situated in the middle of the bilayer at a distance of 4 Å from each other. We used the TIP3P model of water. The valence bonds and angles of water molecules were not fixed. In the starting configuration, water molecules were placed at a distance no less than 2.3 Å from the edge membrane atoms. The degree of solvation was determined as 15 water molecules per hydrocarbon molecule.

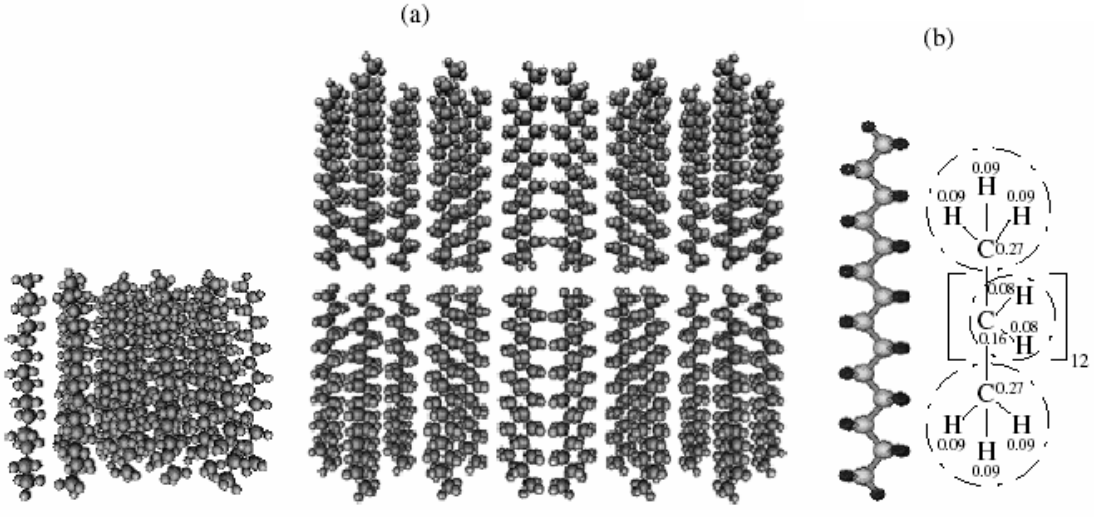

Fig. 1. (*A*) Tetradecane mono- and bilayer and (*B*) charge distribution in the tetradecane molecule (the CH_2 and CH_3 groups are taken to be electrically neutral).

The lipid bilayer was composed of 1-palmitoyl-2-oleoyl-*sn*-glycero-3-phosphatidylcholine (POPC), which contained 64 lipid molecules (Fig. 2). In the initial structure, the direction of the longest molecular dimension was perpendicular to the membrane plane. The initial specific surface area of lipids was 66 Å^2, which was close to the experimental value (62–68 Å^2, [23-26]).

The parameters of potentials for the double bond in oleic residue and partial charges in POPC (Fig. 2 were taken from [6, 27-29]. We used the TIP3P water model; the valence bonds and valence angles in water molecules were not fixed, but were instead determined by the corresponding potentials. In the initial configuration, water molecules were placed at a distance not less than 2.3 Å from the outermost atoms of membranes. The degree of solvation was 44 water molecules per one lipid molecule (full hydration of POPC requires at least 27 water molecules per lipid [30]).

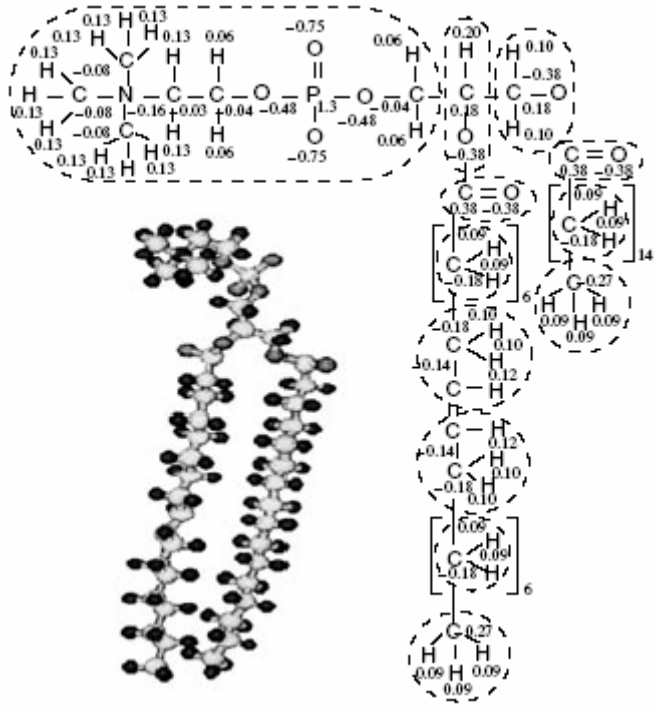

Fig. 2. Charge distribution in a lipid molecule. Electroneutral groups are marked with a dashed line.

The smoothing procedure for Van der Waals interactions involved multiplication of the Lennard-Jones potentials by the smoothing (switching) function *W(r):*

$$W(r)=\begin{cases}1, r \le R_{\text{on}} \\ \dfrac{(R_{\text{off}}^2-r^2)^2(R_{\text{off}}^2-3R_{\text{on}}^2+2r^2)}{(R_{\text{off}}^2-R_{\text{on}}^2)^3}, R_{\text{on}} < r < R_{\text{off}} \\ 0, r \ge R_{\text{off}}\end{cases},$$

where r is the distance between the interacting atoms, R_{on} parameter was 10 and 15 Å, and R_{off} was 10.5 and 16 Å for the tetradecane and lipids, respectively. The Coulomb potential was scaled by the screening function:

$$W(r)=\begin{cases}(1-r/R_{\text{off}})^2, & r \le R_{\text{off}} \\ 0, & r > R_{\text{off}}\end{cases}$$

R_{off} for Van Coulomb interactions was 10 Å in the case of tetradecane membranes and 16 Å in lipid membrane systems. The dielectric constant was assumed to be unity. The step of numeric integration was 1 fs.

Periodic boundary conditions were imposed on the system. Both constant volume *(NVT* ensemble) and constant pressure *(NPT* ensemble) conditions were used for the tetradecane systems. Constant pressure was maintained using a Berendsen barostat [31] with the relaxation time of 100 ps equal in all three directions. In the case of the lipid membrane, the calculations were performed both under the conditions of a constant bilayer area and pressure along the membrane normal (*NPzAT*

ensemble) and under constant pressure in all three directions (NTP ensemble). Constant-pressure condition was achieved by using the Berendsen barostat with equal frequencies in three directions, which varied from 0.1 to 1 ps^{-1}. To consider the effects of the lipid bilayer surface tension, the lateral component of barostatic pressure was assumed to be negative [32]. (It should be kept in mind that, according to the Pascal law, the pressure in the aqueous phase of a system is equal in all directions. Consequently, the real tension pressure in the membrane is somewhat higher than the pressure applied to the water–membrane system.) A virtual collision medium [14] was used for maintaining a constant temperature of 300 K (the temperature of the tetradecane system was also as high as up to 1000 K). The mean frequency of collisions with virtual particles was 10 ps^{-1}, and the mass of virtual particles was 1 amu.

Results and discussion

Tetradecane membranes. At the first stage of calculations, the monolayer was allowed to relax for 200 ps (Fig. 3). The relaxation of the bilayer took nearly the same amount of time.

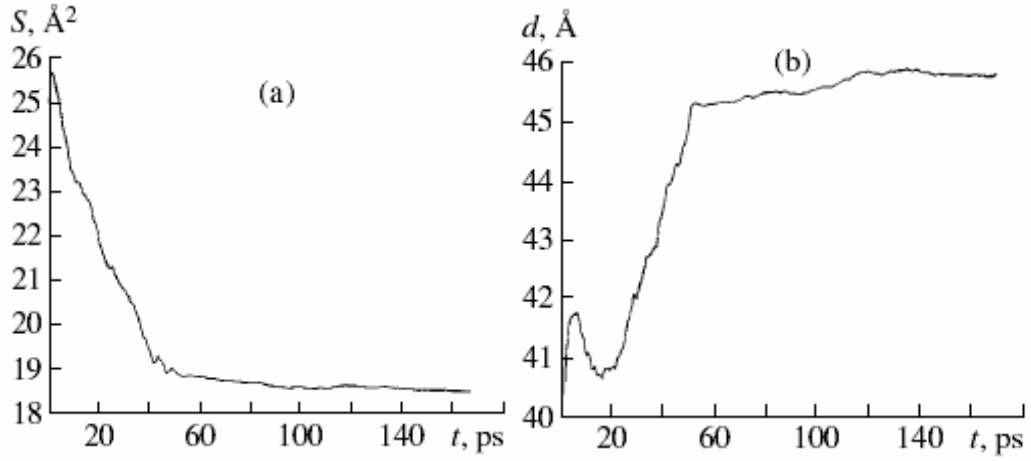

Fig. 3. Relaxation curves for (*A*) specific surface area and (*B*) cell thickness in a system with the tetradecane monolayer.

The hydrophobic properties of several small molecules were studied on the basis of their distribution between two phases, hydrophobic and aqueous.

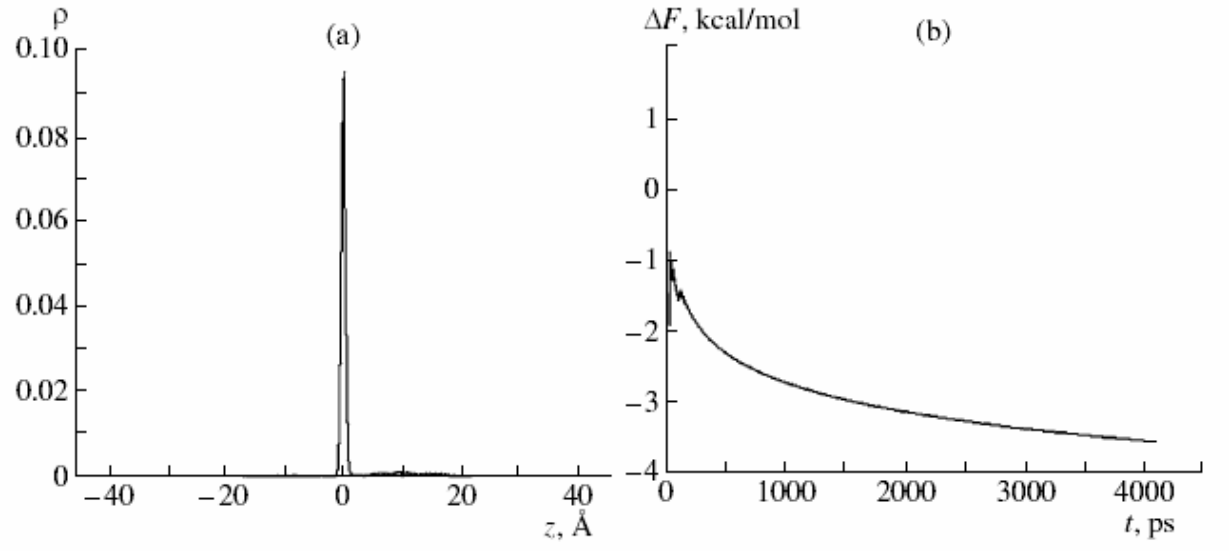

Fig. 4. (*A*) Oxygen molecule distribution between the bilayer and water and (*B*) Gibbs energy of oxygen transfer from water into the bilayer at 300 K and a constant isotropic pressure. See text for the notation.

We studied the dynamics of the diffusion of an oxygen molecule into the tetradecane bilayer. The simulations were performed in the *NVT* and *NPT* ensembles at 300 K. The starting position of the oxygen molecule was at the interphase boundary. The distribution of oxygen between two phases and the Gibbs energy of transfer from water to the bilayer at 300 K and external isotropic pressure 1 atm are shown in Fig. 4.

The free energy of oxygen transfer from water to the membrane at the given volumes of the aqueous and membrane phases was estimated as

$$\Delta F = \lim_{t\to\infty}\Delta F(t) = -kT\lim_{t\to\infty}\ln\frac{\int_{-a/2}^{+a/2}\rho(z,t)dz}{\int_{\varpi}\rho(z,t)dz},$$

where ρ(*z*, *t*) is the probability density function of finding oxygen at a certain position along the *z* axis at the given time instant, +*a*/2 and -*a*/2 are the right and left bilayer boundaries, and the region of integration co was $z > +a/2$ and $z < -a/2$. The free energy of oxygen transfer from water to the hydrophobic zone was more than 3.6 kcal/mol in magnitude; it was determined as a measure of the probability of oxygen molecule occurrence in the bilayer (including the boundary hydrophobic zone, about 3 Å thick) compared with the probability of its occurrence in water. The trajectory length in our numerical experiments was slightly larger than 4 ns. According to experimental estimates, the time of trans-membrane oxygen diffusion in biological membranes is of 50 to 500 ns [33,34].

Figure 4 shows that oxygen penetrates into the membrane in a comparatively short time (<50 ps) and remains there during most of the time of computations; it is predominantly localized in the center of the bilayer, where the largest free volume is. A similar effect was observed in biomembranes in experiments with spin labels [35-37].

The one-dimensional oxygen diffusion coefficient in the direction normal to the membrane, two-dimensional diffusion coefficient in the plane of the bilayer, and three-dimensional diffusion coefficient were calculated as the coefficients of the linear approximations of the curves

$$< z(t)^2 >= 2D_z t\,,$$

$$< x(t)^2 + y(t)^2 >= 4D_{xy} t\,,$$

$$< x(t)^2 + y(t)^2 + z(t)^2 >= 6D_{xyz} t\,,$$

respectively. The angle brackets denote averaging over the whole trajectory. The oxygen diffusion coefficients (cm^2/s) in the bilayer-water system at 300 K and 1 atm are $D_z = 1.71 \times 10^{-5}$, $D_{xy} = 3.09 \times 10^{-5}$, and $D_{xyz} = 2.63 \times 10^{-5}$ for the bilayer and 4.73×10^{-5} for water.

The oxygen diffusion coefficients obtained are in agreement with the known experimental estimates for the diffusion of oxygen in biological membranes, which range from 1.5×10^{-5} to 4.7×10^{-5} cm^2/s [33, 34, 38]. These data are also in agreement with the diffusion coefficients obtained in molecular dynamics calculations (for instance, with the diffusion coefficient in the hexadecane monolayer, 2.6×10^{-5} cm^2/s according to [39]). The calculated oxygen diffusion coefficients in water are more than two times larger than the experimental values for volume diffusion (from 1.76×10^{-5} to 2.3×10^{-5} cm^2/s at 300 K [40-42]). These results are in agreement with the data reported in [43], according to which the self-diffusion coefficient of TIP3P water is also overestimated compared with the experimental value by a factor of more than two. The Stokes-Einstein formula

$$D = k_B T/6\pi\eta r,$$

for the diffusion coefficient of oxygen (η is the viscosity of the solvent and *r* is the radius of the molecule) yields a viscosity of tetradecane in the volume phase of 2.0-2.6 cP [44], which is close to the calculated values.

The distribution of oxygen between the two phases at a constant volume is somewhat different (Fig. 5). The constant volume condition and a comparatively small calculation cell size restrict density

fluctuations in both phases. Oxygen then occurs on the surface of the hydrophobic layer during most of the time.

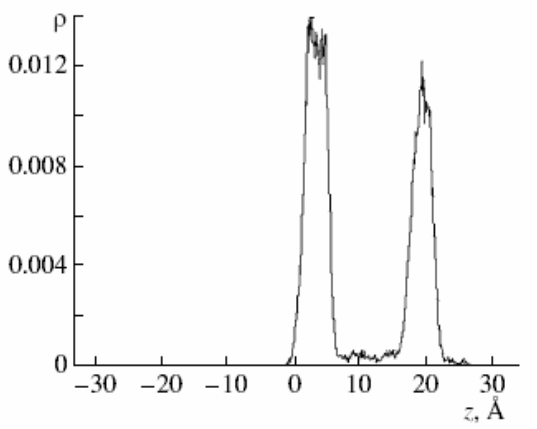

Fig. 5. Oxygen molecule distribution between the bilayer and water at 300 K and a constant volume; the trajectory length is 6 ns.

We also estimated the influence of the charge of a molecule on its distribution between two phases, the tetradecane monolayer and water. We calculated the dynamics of seven types of atoms with partial charges that corresponded to the main types of nonhydrogen atoms of the Amber 1999 force field (Table 1). Such calculations may prove helpful in the development of continual hydrophobic medium models. For instance, interactions with a membrane were modeled in [10] by changes in the potential energy of atoms caused by transfer from the aqueous to hydrophobic phase. These changes were calculated from the transfer energies of amino acids from water to octanol [45]. No complete agreement of the experimental data with the scale of hydrophobicity of amino acids was, however, obtained. According to [11], not only the hydrophobic characteristics of atoms but also the fraction of the surface of atomic spheres exposed to the membrane and aqueous media should be included. We use a simpler model, in which the hydrophobic characteristics of typical force field atoms are calculated from the distribution functions of atoms in the membrane-water system.

We studied the distributions of atomic particles with Amber 1999 force field parameters in the membrane-water system. The charge of atoms of every type was determined by averaging over all possible charges that it had in amino acids taking into account their frequencies of occurrence in proteins [46].

Table 1. Main types of atoms of the Amber 1999 force field.

Atom type	Charge, *e*	r_{VDW}, Å	ε, kcal/mol
C_{aliph}	-0.0463	1.9080	0.1094
C_{aro}	+0.2924	1.9080	0.0860
C_{hetero}	+0.5382	1.9080	0.0860
N	-0.4698	1.8240	0.1700
O	-0.3180	1.7210	0.2104
O*	-0.6137	1.6612	0.2100
S	-0.2525	2.0000	0.2500

Table 1 contains the effective charges of atoms, their Van der Waals radii, and the energy parameters of Van der Waals interactions. Trajectories 5 to 7 ns long were calculated. The calculations

were performed for the *NVT* ensemble at 1000 K to accelerate the procedure of configuration space scanning.

The distributions of the most hydrophobic and most hydrophilic ions are shown in Fig. 6 (the upper and lower rows, respectively). As expected, the ions with lower charges were more hydrophobic.

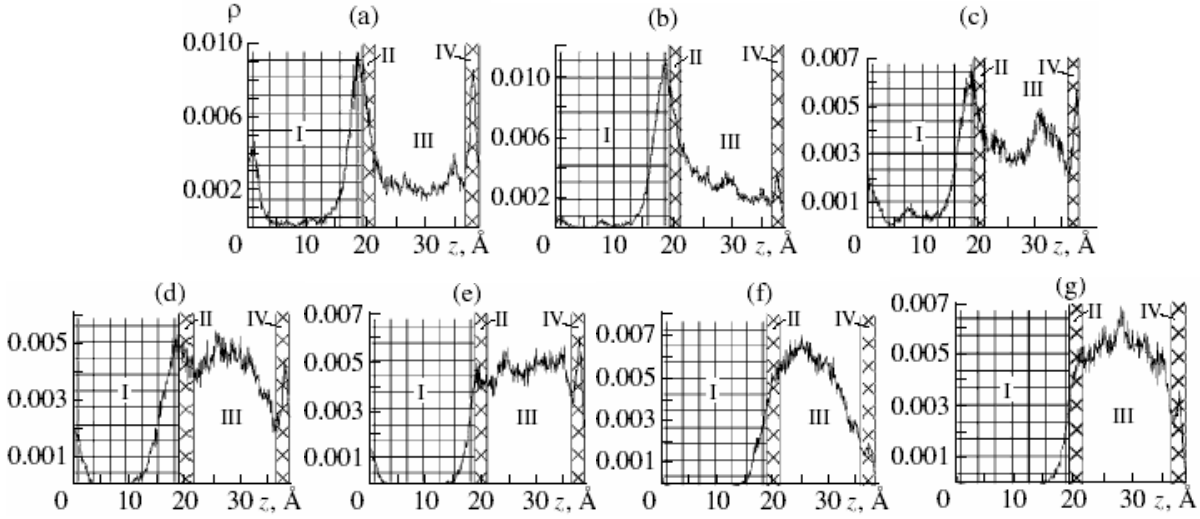

Fig. 6. Distribution profiles for the atoms (*A*) C_{aliph}, (*B*) S, (*C*) C_{arom}, (*D*) O, (*E*) N, (*F*) O*, and (*G*) C_{hetero}. Order of zones: (I) hydrocarbon monolayer, (II) surface hydrophobic layer, (III) aqueous layer, and (IV) surface hydrophobic layer (on the opposite side of the hydrocarbon monolayer).

Note that the ratio between the charge *z* and hydro-phobic properties of an ion can be estimated from the Born theory, which also takes into account the ion size *r*. According to this theory, the change in the electrostatic component of the Gibbs energy caused by the transfer of an ion from water into a membrane layer can be estimated as

$$\Delta W_{\mathrm{B}} = \frac{z^2 e^2}{8\pi r \varepsilon_0}\left(\frac{1}{\varepsilon_2} - \frac{1}{\varepsilon_1}\right)$$

where ε_1 and ε_2 are the relative permittivities of water and the non-polar solvent $\varepsilon_1 \sim 80$ and $\varepsilon_2 \sim 2$-3).

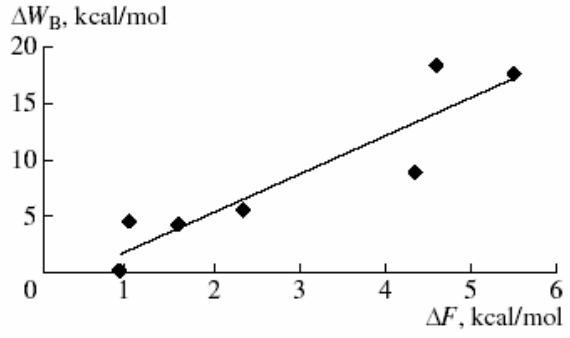

Fig. 7. Correlation between the calculated energy of transfer and the corresponding Born energy for seven types of atoms; correlation coefficient 0.9167.

The calculated free energies of transfer of atoms from water into the monolayer correlate with changes in the Born energy (Fig. 7). Ions with lower charges and larger diameters are more strongly stabilized in the membrane. These results are in agreement with the experimental data on the penetration of ions through the water-oil interphase boundary, which correlate well with Born solvation energies [47].

Special calculations showed that the contributions of separate atoms to the distribution of functional groups were not additive (cf. Figs. 6 and 8). For instance, the distribution of the CO group was not the sum of the distributions of C_{hetero} and O*, which constitute the CO group. For CO, the likely reason for this is the appearance of a dipole moment when the group is formed. It follows that the possibility of using a simple model based on the introduction of some specific hydrophobic characteristic for every type of atom proves to be very problematic.

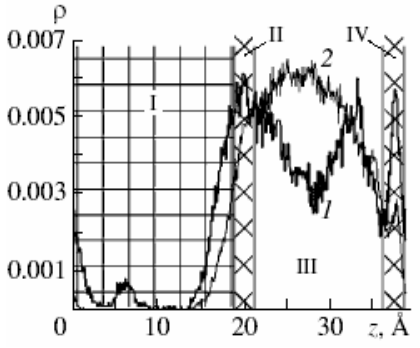

Fig. 8. (*1*) CO group distribution profile and (*2*) the sum of distribution profiles for the C_{hetero} and O atoms; trajectory length 5 ns. See Fig. 6 for zone denotations (I-IV).

We also considered the distributions between water and the hydrocarbon phase of six amino acid residues with different polarities (Ala, Asp, Gly, Phe, Trp, and Val) at 300 K. The cell with the hydrated tetradecane monolayer was then maintained at a constant pressure of 1 atm. The specific surface area per tetradecane molecule was 18.2 $Å^2$. The starting position of the amino acids was at the monolayer boundary. The plots of the distribution of the residues are given in Fig. 9. None of the residues succeeded in penetrating into the mono-layer during 10 ns of computations. This shows that, at the given membrane density, the interphase boundary is a serious obstacle to the penetration of amino acid residues.

The energy of amino acid transfer from water to octanol [45] is frequently used as a measure of the hydrophobic properties of the corresponding residues. Applying this criterion, we find that the most hydro-phobic amino acid residues concentrate at the tetradecane boundary, whereas more hydrophilic residues reside in the aqueous phase during a somewhat longer time.

The calculations described above were performed under equilibrium conditions. At the same time, non-equilibrium dynamics methods are currently being developed to handle nonequilibrium systems. We also developed an approach to the dynamics of membrane structure that uses nonequilibrium steered dynamics methods. Additional external forces (constant or varying with time) then act on separate atoms.

We studied the dynamics of model spheres that interacted with the other atoms only by Van der Waals forces. The force applied to a probe particle was a sine function of time and was directed normally to the membrane. The mean force value was set at 1 to 10 kcal/(Å mol) (1 kcal/(Å mol) ≈ 70 pN).

Our numerical experiment showed that spheres of radii 2 and 4 Å moved in the TIP3P aqueous medium at velocities of 10 and 2.6 Å/ps, respectively, at a constant external force of 10 kcal/(Å mol). That is, the Stokes law was likely violated slightly at particle radii smaller than or close to the radius of medium molecules. When a particle of radius 2 Å moves, the effective viscosity of the medium is approximately two times lower than for large particles.

We studied the penetration of particles under the action of an external force through the membrane layer. Probe spheres penetrated through the layer in time of about 2.5 ns under the action of a force whose mean value was no less than 7 kcal/(Å mol) (Table 2).

A substantial decrease in the time of repeat penetrations shows that pore formation plays a decisive role in penetration through the tetradecane monolayer. Forcing a sphere through a monolayer results in the formation of a pore and deformation of the surrounding membrane structure. The relaxation time of such a pore is comparatively long. For instance, after a series of many particle passages under the action of a constant force of 10 kcal/(Å mol) (Table 2), the last passage took time as short as 9 ps. Shifting the probe

sphere in the plane of the membrane by a distance equal to its radius increased the passage time to 12 ps; for a distance equal to the diameter, the time of passage increased a bit, to 20 ps.

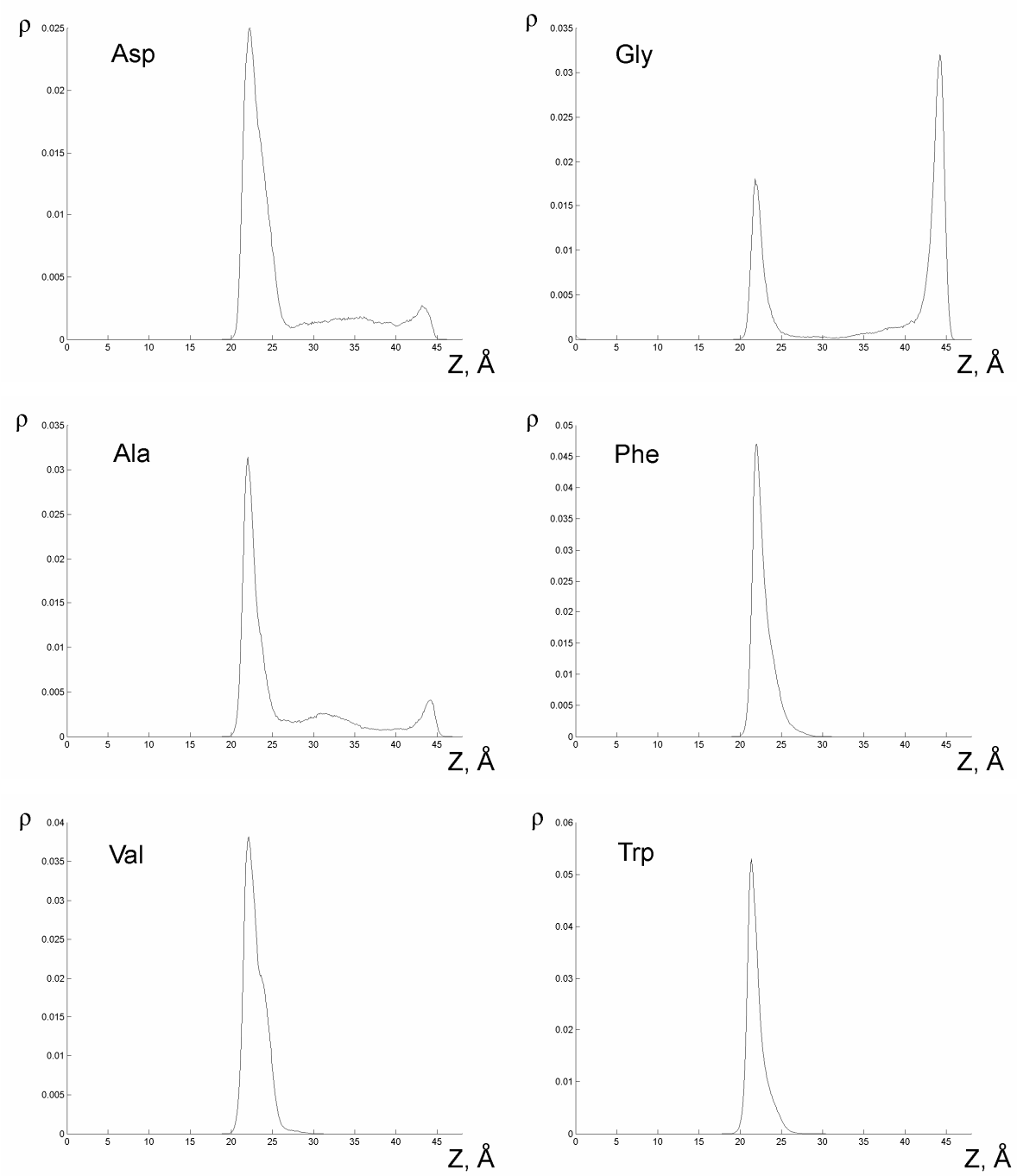

Fig. 9. Distribution density of an amino acid residue along the normal to the membrane *z* averaged over atoms (averaging is performed with weight factors proportional to atomic weights). The order in which the plots are arranged (from left to right and from top to bottom) corresponds to decreasing the Gibbs energy of amino acid transfer from water to octanol. Monolayer boundaries along the z axis are z = 0 and 20 Å (taking into account periodic boundary conditions, *z* = 46 Å is also a monolayer boundary); the aqueous phase occupies space between 20 and 46 Å.

Table 2. Characteristic times of passage through the membrane under the action of a periodic force $F(t) = \bar{F}_0 + C_0\sin(2\pi t/T)$, where $C_0 = 2$ kcal/Å/mol, for $\bar{F}_0 = 7$ and 10 kcal/Å/mol; at $T = \infty$, $F(t) = \bar{F}_0 = \text{const}$; particle radius 4 Å.

$\bar{F}_0$, kcal/(Å mol)	T, ps	τ_1, ps	$\bar{\tau}$, ps	$\bar{\tau}_2$, ps
7	0.1	> 2500	–	–
7	1	1268	214	108
7	∞	724	149	101
10	0.1	155	15	13
10	1	1547	48	15
10	∞	1899	173	29

Note: $\bar{F}_0$ is the mean external force, T is the period, τ_1 is the time of the first passage, $\bar{\tau}$ is the mean time of all passages, and $\bar{\tau}_2$ is the mean time of all except the first passages.

The forced transport of a probe molecule in a medium at the parameter values under consideration does not depend linearly on the force applied. We also did not observe resonance effects over the range of external force frequency variations that we studied.

Table 3. Time of passage of molecules of various diameters through the membrane under the action of a constant force (F_0)

F_0, kcal/(Å mol)	R_0, Å	τ_1, ps	$\bar{\tau}$, ps	$\bar{\tau}_2$, ps
7	3.1	660	25	16
7	4	724	149	101
10	3.1	21	18	15
10	4	1899	173	29

Note: R_0 is the effective radius of the molecule; see Table 2 for the other notation.

A comparison of the directed movement of a sphere of radius 4 Å and the alanine residue of effective radius 3.1 Å (Table 3) through a layer of tetradecane shows that increasing the force is not accompanied by a proportional increase in the rate of repeat alanine passages through the membrane. For the sphere, an increase in the rate is essentially nonlinear. Note that, unlike a sphere, the alanine residue is flexible to a certain degree. It appears that the degree of membrane deformation and activation barrier values related to pore formation are quite different for spheres and alanine residues.

POPC bilayer. The POPC bilayer was subjected to multistep equilibration. Preliminary equilibration of the bilayer was performed at T= 300 K and isotropic barostating at 1 atm (barostatic frequency, 0.2 ps^{-1}). Then, the membrane was deliberately stretched by linear increase in the lateral dimensions of simulation box. This technical approach allowed us to set the system into a state in which the area of the membrane corresponded to the experimental value. Then, the system was further equilibrated for 750 ps under *NPzAT*-conditions. Mean lateral pressure component at

this part of the trajectory was -330 atm. The mean membrane normal component was -118 atm. Total equilibration time was 1 ns (then followed by the operative region of the trajectory; in the other cases, the duration of equilibration is implicitly stated). At the working part of the trajectory, we performed barostating at a frequency of 1 ps^{-1} and a mean pressure of $P_x = P_y$ = -260 atm in the *XY* plane (which is parallel to the membrane plane) and P_z = 1 atm in the normal direction.

After the equilibration, basic membrane characteristics such as surface tension, surface density of lipids, radial distribution functions of atoms in the bilayer plane, the thickness of bilayer, distribution of atomic groups along the membrane normal, and parameters of order for lipid chains agree in general with the data obtained in other computer investigations and experimental data [3, 23-26, 48-56].

Heterogeneity of the membrane system affects its interactions with penetrant molecules. For computation of parameters which determine diffusion of molecules in the membrane, we used the SMD method [18, 19]. External forces (constant and alternating) were applied to some parts of the system. We used testing spheres of 18 amu with radii of 2 and 4 Å (i.e., an order of the radius of the carbon atom and a small functional group, respectively), which interact with the other atoms only by Van der Waals forces (interaction constant ε, 0.15 kcal/mol). Constant external force F_{ext} was applied along the normal or in the membrane plane. In the first case, the testing sphere was preliminary fixed at 2 Å from the membrane; in the second case, it was placed in the center of the membrane, before the membrane was equilibrated for 2 ps. Then, we applied a force of 0.3 kcal/mol $Å^{-1}$ to 4 kcal/mol $Å^{-1}$ (1 kcal/mol $Å^{-1}$ = 7 × 10^{-6} dyn). In the case of the 2-Å sphere, the force value was 10 kcal/mol $Å^{-1}$ (Fig. 10).

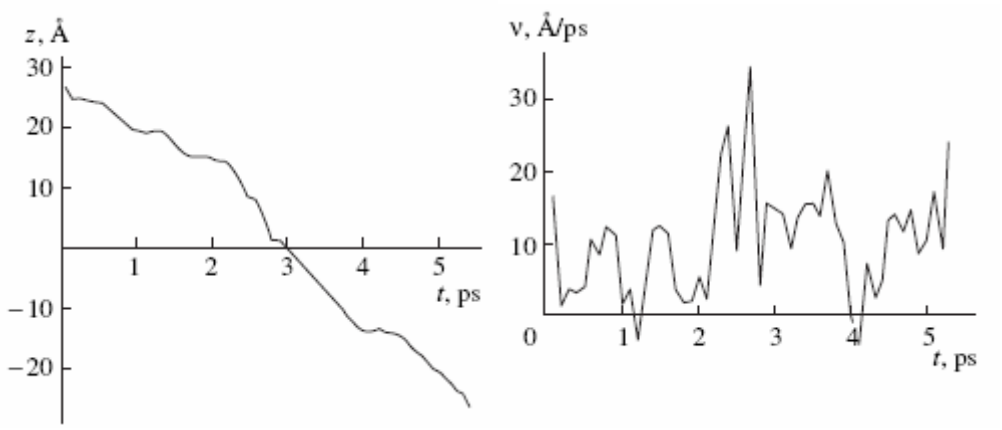

Fig. 10. Kinetics of movement of the testing Van der Waals 2-Å sphere, subjected to a force of 10 kcal/mol $Å^{-1}$ applied in the direction of the normal. (*A*) Position of the sphere on the Z axis (normal to the membrane). The center of the bilayer is located at z = 0; the borders, at z =±20 Å. (*B*) The velocity of sphere movement averaged over an interval of 0.1 ps.

According to the test simulations, a constant force of 10 kcal/mol $Å^{-1}$ drives the 2- and 4-Å spheres in the TIP3P water with mean velocities of 10 and 2.6 Å/ps, respectively. The deviation from the hydrodynamic Stokes equation had two causes. First, the particle radii exceeded the range of applicability of the continuous medium approximation. Second, the value of applied force and, consequently, the motion velocity were relatively high, and the condition of laminar flow did not hold either. However, the Stokes equation could also provide valid qualitative estimates at the microlevel [57]. Calculation of the SMD trajectories in the membrane system was stopped when the first Van der Waals sphere permeated through the membrane, but for no longer than 2 ns. At forces of 1–10 kcal/mol $Å^{-1}$, the 2-Å spheres penetrated through the membrane in less than 2 ns. In the other cases, the spheres got stuck at the surface or penetrated into the membrane layer only to a certain depth. At forces below 1 kcal/mol $Å^{-1}$, the influence of perturbation of the medium on the 4-

Å sphere was comparable to the effect of the applied force and, in some cases, the testing molecule also deviated from the initial position, away from the membrane, to distances up to 2 Å.

At the above-critical forces (for instance, 1 kcal/mol $Å^{-1}$ for a 2-Å sphere), the molecules penetrated the membrane relatively rapidly. The penetration velocity in this case is determined mainly by the external force, whereas the diffusion contribution is relatively low.

The values of laterally applied forces F_{ext} were 1, 2, 4, and 10 kcal/mol $Å^{-1}$. For F_{ext} = 1 kcal/mol $Å^{-1}$, we analyzed the kinetic characteristics at the 75-ps part of the trajectory, when the particle remained at the center of the bilayer.

The coefficient of viscous friction γ was defined as the ratio of external force to the velocity of particle drift:

$$\gamma = \frac{F_{ext}}{v}.$$

Formally, the friction coefficient could be redefined in terms of diffusion coefficient, using the known Einstein relation, and in terms of microviscosity of the medium using the Stokes equation. It is noteworthy that in this case the Stokes equation is inapplicable. As to the Einstein relation, a special study is needed to verify its applicability in this particular situation, which is beyond the scope of this paper.

Currently, limited data are available on the viscosity when a particle moves along the normal to membrane surface or in the lateral direction in the middle of the bilayer. Experimental averaged viscosities of the surface layer range from 30 to 190 cP in various lipid membranes [58-60]. The experimental estimate of the mean viscosity of POPC is about 18 cP [61]. Since the micro viscosities are not the same in different regions of the membrane, it is reasonable to define several structurally and dynamically inhomogeneous regions. In the first approximation, one can distinguish the regions of lipid head-groups and alkyl chains. Fig. 11 shows the friction coefficients in terms of microviscosity for various regions of the system plotted against the external force applied to a 2-Å particle in the direction of the normal to the membrane plane.

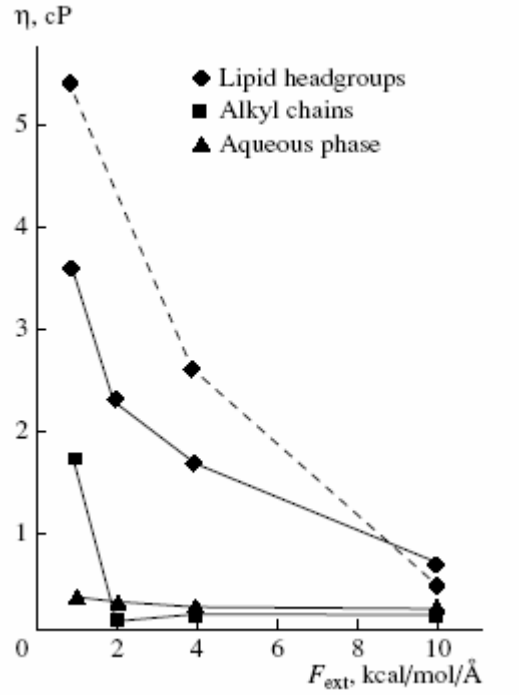

Fig. 11. Effective microviscosity in the POPC-water system. The radius of the testing Van der Waals sphere is 2 Å. The solid line shows the system after preliminary equilibration for 500 ps; the dashed line, after complete equilibration for 1 ns.

Calculated values of effective viscosity of water for a 2-Å sphere are 0.3–0.4 cP, which is two to three times lower than the experimental values. These data agree with the known estimates of water viscosity for the TIP3P model [43]. Transverse viscosity of the membrane does not exceed 6 cP. Viscosity of the central part of the bilayer is several times lower than this value.

Data on the lateral movement of the sphere under influence of force are presented in Fig. 12. In this case, the effective microviscosity is very close to that measured in the region of alkyl tails in the direction of the normal.

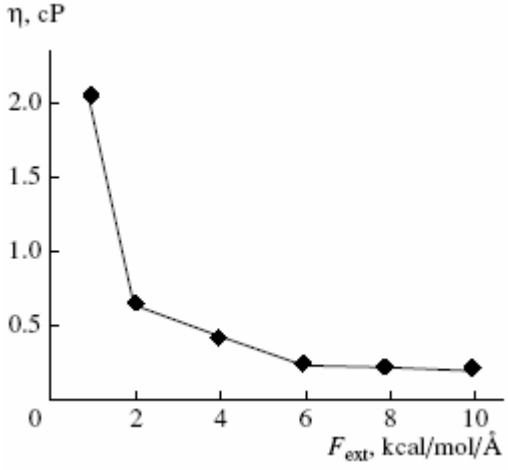

Fig. 12. Effective microviscosity in the center of the POPC bilayer. The radius of testing Van der Waals sphere is 2 Å.

It is noteworthy that for 2-Å particles, the Stokes equation in the region of alkyl tails is almost inapplicable. In general, the results suggest a non-Newtonian character of the medium and a weakly nonequilibrium state of this system at movement velocities of 1–10 Å/ps.

The velocity of penetration of the molecule under the influence of external force also depends on the chemical properties of the molecule. For comparison, we calculated the dynamics of penetration of tryptophan (effective radius, 4.8 Å) and alanine residues (effective radius, 3.1 Å), as well as of the 2-Å Van der Waals sphere, into the bilayer. The obtained values of effective microviscosity are shown in Fig. 13. In the case of many-atom molecules, the force was applied uniformly to all the atoms of the system.

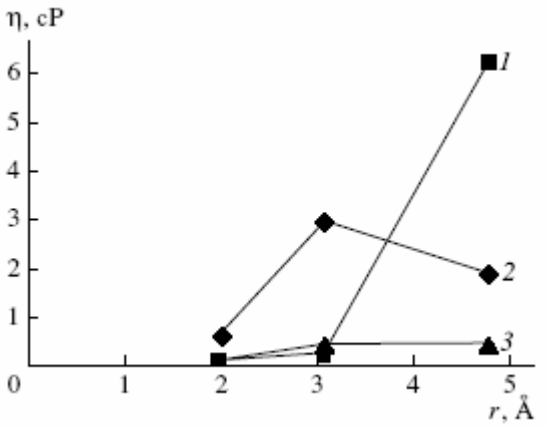

Fig. 13. Dependence of microviscosity on the effective radii of testing molecules in the POPC–water system. Total F_{ext}= 10 kcal/mol Å^{-1}. Notations: *1,* alkyl chains; 2, lipid head-groups; *3,* aqueous phase.

It should be noted that a more polar tryptophan residue has a higher velocity in the region of lipid head-groups than the alanine residue, which, consequently, provides a lower value of

microviscosity. In the region of hydrophobic alkyl chains, the situation is the reverse, with velocities differing by a factor of 15. The region of lipid head-groups is most sensitive to the nature of a molecule moving through the membrane. Conversely, the hydrophobic core of the bilayer with a larger free volume is sensitive to the size of particles.

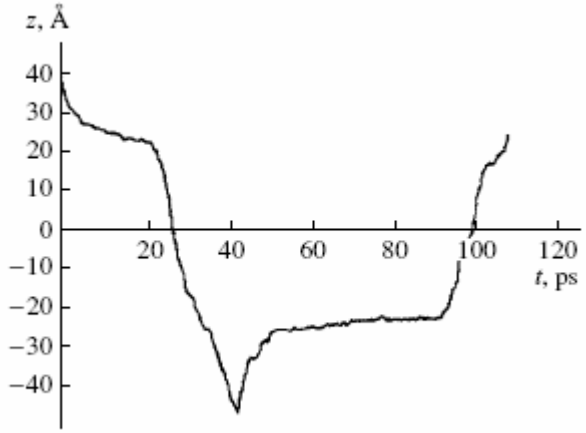

Fig. 14. Dynamics of movement of alanine residue through the lipid membrane. The position of the geometric center of the residue is shown. The borders of bilayer are located at +22 Å. At the point of sharp bend of the curve, the direction of the force was inverted.

An example of forced transmembrane transport of alanine residue (Fig. 14) allows us to reveal the presence of factors facilitating recurring transmembrane movement related to the effects of structural memory in the bilayer. Pore formation, which accompanies molecule movement through the tetradecane monolayer, was studied in the previous subsection. The effect of formation of a long-living pore in lipid membranes was not observed at the same values of external force. Both before and after the first translocation through the membrane, alanine residue spends a certain time in the adsorbed state and then rapidly (compared to the movement in the water phase) passes through the membrane.

Summary

1. Spontaneous diffusion in tetradecane membranes. The simplest full-atomic model of a hydrated organic membrane structure used in this work allows us to study the laws that govern the distribution of various molecules between two phases, hydrophobic structured and aqueous. We showed that only very small and strongly hydrophobic molecules, for instance, oxygen, can penetrate on their own into a membrane layer under normal conditions in times shorter than 10 ns. At a fixed volume, penetration into a structured membrane medium is strongly impeded. We observed oxygen accumulation in the middle of the bilayer, which was caused by increased looseness of the structure at the interface between two monolayers.

A study of the dynamics of spontaneous transmembrane diffusion in times on order of 10 ns requires calculations at elevated temperatures. The free energy of transfer calculated at 1000 K for the main types of Amber 1999 atoms varies from 0.9 to 5.5 kcal/mol. These energy changes well correlate with changes in the corresponding Born solvation energies. The Helmholtz energy of transfer increases (that is, hydrophobic properties weaken) in the series of atoms C_{aliph}, S, C_{arom}, O, N, O*, C_{hetero}. Importantly, atomic contributions to the free energy of transfer of functional groups are not additive. This impedes the continual simulation of hydrophobic media by including an additional term describing the interaction of atoms with this medium into the potential energy.

The calculated distributions of amino acid residues between phases are in conformity with their known hydrophobic properties. Note that, under the specified conditions of calculations, a membrane is a very substantial barrier to the penetration of amino acid residues into it.

2. Steered diffusion in tetradecane membranes. A consideration of equilibrium dynamics processes of even comparatively small molecules in such a system does not allow us to draw final conclusions on the balance of hydrophobic forces at room temperature at the expense of reasonable computing time expenditures. The steered dynamics method that we are developing can be used to organize a directed and faster scenario of the development of events for certain degrees of freedom. The kinetic coefficients calculated this way are related to the equilibrium parameters of the system by thermodynamic and statistical equations. The degree to which the system is nonequilibrium should then, however, be controlled. For instance, nonlinear dependences of the velocities of directed molecule movements on the external force value appear already at velocities of 1 Å/ps. Special studies of the reasons for this effect (weakly nonequilibrium state of the system and (or) the non-Newtonian character of the medium) are beyond the scope of this work. The same is true of the dynamics of formation and relaxation of supramolecular membrane structures (pores in the context of this work). The formation of a pore dramatically changes the dynamics of transmembrane transport. The relaxation time of a pore in the membrane under study is comparatively long (more than 10 ps), and memory effects in the dynamics of membranes can be very significant.

3. Dynamic heterogeneity of lipid membranes. In this paper, we also developed the method of "computer viscosimetry", which makes it possible to reveal the difference in diffusive properties of various molecules and to determine the effective viscosity characteristics in microheterogeneous structures, which are difficult to measure in conventional experiments. It should be noted that the very terms viscosity and micro viscosity in such systems require specific clarifications. In fact, we consider a quantitative characteristic of local dissipative properties expressed in units of viscosity. The hydrodynamic Stokes equation can only be used for estimating the order of magnitude of this characteristic. In this case, calibration of micro viscosity in a defined range of forces is required for particles of particular size and chemical composition.

Anisotropic microviscosity in different regions of the lipid bilayer can vary by an order of magnitude or even more. Considerable velocities of molecule penetration into the bilayer on the time scale of about 2 ns were found only when the value of external force is above a critical value. The critical force value increases with the radius of the molecule. Again, nonequilibrium effects appear at velocities exceeding 1 Å/ps.

The greatest difference in effective microviscosity of the lipid bilayer, depending on the chemical nature of the penetrant molecule, was found in the region of lipid head-groups.

The friction coefficients in the lipid membrane normal direction, obtained for the above-critical forces value (approximately 1 kcal/mol/ Å), do not exceed 6 cP in terms of effective microviscosity. The viscosity of the central region of the bilayer for the Van der Waals sphere was found to be an order of magnitude lower than that of the surface region. At forces exceeding the critical value, there is a time delay in particle penetration into the membrane, the delay decreasing with an increase in the force. The viscosity of the central region of the lipid bilayer in the lateral direction was close to the viscosity of the region of alkyl chains, when the force is applied in the direction of the normal.

The work was supported by RF Federal Agency on Science and Innovation, RF Federal Agency on Education, Russian Foundation for Basic Research (projects no. 04-04-49645, 06-04-08136) and US CRDF (2803).

References

[1] S.Tristram-Nagle, H.I.Petrache and J.F.Nagle: Biophys. J. 75 (1998), pp. 917-925.

[2] S.Tristram-Nagle, Y.Liu, J.Legleiter and J.F.Nagle: Biophys. J. 83 (2002), pp. 3324-3335.

[3] H.Heller, M.Schaefer and K.Schulten: J. Phys. Chem. 97 (1993), pp. 8343-8360.

[4] K.V.Shaitan and P.P.Pustoshilov: Biophysics (transl. from Russ.) 44 (1999), pp. 429-434.

[5] N.K.Balabaev, A.L.Rabinovich, P.O.Ripatti and V.V.Kornilov: Russ. J. Phys. Chem. (transl. from Russ.) 72 (1998), pp. 595-598.

[6] A.L.Rabinovich, P.O.Ripatti and N.K.Balabaev: J. Biol. Phys. 25 (1999), pp. 245-262.

[7] A.L.Rabinovich, P.O.Ripatti, N.K.Balabaev and F.A.M.Leermakers: Phys. Rev. E 67 (2003), p. 011909.

[8] F.A.M.Leermakers, A.L.Rabinovich and N.K.Balabaev: Phys. Rev. E 67 (2003), p. 011910.

[9] A.L.Rabinovich, P.O.Ripatti and N.K.Balabaev: Russ. J. Phys. Chem. (transl. from Russ.) 76 (2002), pp. 1824-1828.

[10] O.Edholm and F.Jänig: Biophys. Chem. 30 (1998), pp. 279-292.

[11] R.G.Efremov, P.E.Volynsky, D.E.Nolde, G.Vergoten and A.S.Arseniev: Theor. Chem. Acc. 106 (2001), pp. 48-54.

[12] D.P.Tieleman, S.J.Marrink and H.J.Berendsen: Biochim. Biophys. Acta 1331 (1997), pp. 235-270.

[13] A.S.Lemak and N.K.Balabaev: Mol. Simul. 15 (1995), pp. 223-231.

[14] A.S.Lemak and N.K.Balabaev: J. Comput. Chem. 17 (1996), pp. 1685-1695.

[15] K.V.Shaitan and S.S.Saraikin: Russ. J. Phys. Chem. (transl. from Russ.) Vol. 76 (2002), pp. 987-992.

[16] V.L.Golo and K.V.Shaitan: Biophysics (transl. from Russ.) 47 (2002), pp. 567-573.

[17] V.L.Golo, V.N.Salnikov and K.V.Shaitan: Phys. Rev. E 70 (2004), p. 046130.

[18] S.Park and K.Schulten: J. Chem. Phys. 120 (2004), pp. 5946-5961.

[19] B.Isralewitz, M.Gao and K.Schulten: Curr. Opin. Struct. Biol. 11 (2001), pp. 224-230.

[20] K.V.Shaitan: Biophysics (transl. from Russ.) 39 (1994), pp. 993-1011.

[21] K.V.Shaitan, M.D.Ermolaeva, N.K.Balabaev, A.S.Lemak and M.V.Orlov: Biophysics 42 (1997), pp. 558-566.

[22] J.Wang, P.Cieplak and P.A.Kollman: J. Comput. Chem. 21 (2000), pp. 1049-1074.

[23] P.A.Hyslop, B.Morel and R.D.Sauerheber: Biochemistry1990), pp. 1025-1038.

[24] G.Pabst, M.Rappolt, H.Amenitsch and P.Laggner: Phys. Rev. E 62 (2000), pp. 4000-4009.

[25] J.M.Smaby, M.M.Mornsen, H.L.Brockman and R.E.Brown: Biophys. J. 73 (1997), pp. 1492-1505.

[26] R.W.Evans, M.A.Williams and J.Tinoco: Biochem. J. 245 (1987), pp. 455-462.

[27] T.R.Stouch, K.B.Ward, A.Altieri and A.T.Hagler: J. Comput. Chem. 12 (1991), pp. 1033-1046.

[28] S.E.Feller, D.Yin, R.W.Pastor and A.D.Mackerell, Jr.: Biophys. J. 73 (1997), pp. 2269-2279.

[29] M.Schlenkrich, J.Brickmann, A.D.Mackerell, Jr. and M.Karplus, in *Biological membranes: a molecular perspective from computation and experiment*, edited by K. M. Merz, Jr. and B. Roux, Birkhauser, Boston (1996).

[30] K.Murzyn, T.Ryg, G.Jezierski, Y.Takaoka and M.Pasenkiewicz-Gierula: Biophys. J. 81 (2001), pp. 170-183.

[31] H.J.C.Berendsen, J.P.M.Postma, W.F.van Gunsteren, A.DiNola and J.R.Haak: J. Chem. Phys. 81 (1984), pp. 3684-3690.

[32] S.W.Chiu, M.Clark, V.Balaji, S.Subramaniam, H.L.Scott and E.Jakobsson: Biophys. J. 69 (1995), pp. 1230-1245.

[33] A.Lavi, H.Weitman, R.T.Holmes, K.M.Smith and B.Ehrenberg: Biophys. J. 82 (2002), pp. 2101-2110.

[34] M.Roslaniec, H.Weitman, D.Freedman, Y.Mazur and B.Ehrenberg: J. Photochem. Photobiol. B 57 (2000), pp. 149-158.

[35] A.Ligeza, A.N.Tikhonov, J.S.Hyde and W.K.Subczynski: Biochim. Biophys. Acta 1365 (1998), pp. 453-463.

[36] D.Marsh: Proc. Natl. Acad. Sci. USA 98 (2001), pp. 7777-7782.

[37] B.G.Dzikovski, V.A.Livshits and D.Marsh: Biophys. J. 85 (2003), pp. 1005-1012.

[38] M.W.Merx, U.Flögel, T.Stumpe, A.Gödecke, U.K.Decking and J.Schrader: FASEB J. 15 (2001), pp. 1077-1079.

[39] S.J.McKinnon, S.L.Whittenburg and B.Brooks: J. Phys. Chem. 96 (1992), p. 10506.

[40] S.Th.Bouwer, L.Hoofd and F.Kreuzer: Biochim. Biophys. Acta: Prot. Struct. Mol. Enzym.1997), pp. 127-136.

[41] T.Itoh, K.Yaegashi, T.Kosaka and H.Fukushima: Biorheology 33 (1996), p. 80.

[42] C.E.St-Denis and C.J.Fell: Canad. J. Chem. Eng. 49 (1971), p. 885.

[43] M.W.Mahoney and W.L.Jorgensen: J. Chem. Phys. 114 (2001), pp. 363-366.

[44] H.S.Park, T.Chang and S.H.Lee: J. Chem. Phys. 113 (2000), pp. 5502-5510.

[45] J.L.Fauchère and V.Pliska: Eur. J. Med. Chem. Chim. Ther. 18 (1986), pp. 369-375.

[46] G.E.Schulz and R.H.Schirmer, Principles of protein structure, Springer-Verlag, New York–Heidelberg-Berlin 1979.

[47] K.Wu, M.J.Iedema and J.P.Cowin: Science 286 (1999), pp. 2482-2485.

[48] Ye.V.Tourleigh, K.V.Shaitan and N.K.Balabaev: Biologicheskie Membrany (in Russ.) 22 (2005), pp. 491-502.

[49] R.Rand and V.Parsegian: Biochim. Biophys. Acta 998 (1989), pp. 351-376.

[50] G.Pabst: Langmuir 16 (2000), pp. 8994-9001.

[51] Z.Salamon, G.Lindblom, L.Rilfors, K.Linde and G.Tollin: Biophys. J. 78 (2000), pp. 1400-1412.

[52] J.Seelig and A.Seelig: Q. Rev. Bioph. 13 (1980), pp. 19-61.

[53] D.Huster, P.Müler, K.Arnold and A.Herrmann: Biophys. J. 80 (2001).

[54] M.Lafleur, P.R.Cullis and M.Bloom: Eur. Biophys. J. 19 (1990), pp. 55-62.

[55] M.J.Schneider and S.E.Feller: J. Phys. Chem. B 105 (2001), pp. 1331-1337.

[56] R.A.Böckmann, A.Hac, T.Heimburg and H.Grubmüller: Biophys. J. 85 (2003), pp. 1647-1655.

[57] G.K.Batchelor, in *Theoretical and Applied Mechanics. IUTAM Congress*, edited by W. T. Koiter, North Holland-Elsevier Science Publishers, Amsterdam–New York–Oxford (1976).

[58] C.E.Kung and J.K.Reed: Biochemistry 25 (1986), pp. 6114-6121.

[59] W.R.Dunham, R.H.Sands, S.B.Klein, E.A.Duelli, L.M.Rhodes and C.L.Marcelo: Spectrochim. Acta A 52 (1996), pp. 1357-1368.

[60] M.Sinensky: Proc. Natl. Acad. Sci. USA 71 (1974), pp. 522-525.

[61] A.Sonnleitner, G.J.Schütz and Th.Schmidt: Biophys. J. 77 (1999), pp. 2638-2642.